568781
P30

NASA Technical Memorandum 101687

THERMAL/STRUCTURAL ANALYSIS OF THE SHAFT DISK REGION OF A FAN DRIVE SYSTEM

Peyton B. Gregory and Anne D. Holland

ORIGINAL CONTAINS
COLOR ILLUSTRATIONS

MARCH 1990

(NASA-TM-101687) THERMAL/STRUCTURAL ANALYSIS OF THE SHAFT-DISK REGION OF A FAN DRIVE SYSTEM (NASA) 29 p CSCL 20K

N90-22807

Unclas
G3/39 0269658

National Aeronautics and
Space Administration

Langley Research Center
Hampton, Virginia 23665-5225

ORIGINAL CONTAINS
COLOR ILLUSTRATIONS

THERMAL/STRUCTURAL ANALYSIS OF THE SHAFT DISK REGION OF A FAN DRIVE SYSTEM

by Peyton B. Gregory and Anne D. Holland

Langley Research Center

INTRODUCTION

In January 1989, a mishap occurred in the National Transonic Facility wind tunnel at NASA Langley Research Center. The most probable cause of this mishap was the failure of an insulation retainer, shown in figure 1, which holds the foam insulation around the fan drive shaft. Failure of this retainer resulted in the subsequent damage to other components in the tunnel. The analysis of the insulation retainer (reference 1) indicated that the component was highly stressed which gave it a limited cycle life. The purpose of the insulation was to reduce the thermal stresses in the shaft at the shaft-disk interface during a cryogenic run.

The objective of this analysis is to determine the effect of removing this external thermal insulation on the stresses in the shaft, disk and bolts holding the two together. To accomplish this, a detailed thermal/structural finite element analysis of the shaft-disk interface was performed using PATRAN (reference 2) model development and EAL (reference 3) analysis software. The maximum stresses on the three components were determined for several conditions with and without the external thermal insulation. These results were compared to the original analyses to assess the effect based on the proposed future operation of the shaft-disk structures of the fan drive system.

COMPONENT DESCRIPTION

The fan drive system assembly in the area of the shaft-disk interface is shown in figure 1. The disk is a 156.0 inch diameter forging with an 18.0 inch diameter bore hole in the center. At the bore hole, it is 8.0 inches thick tapering radially outward to produce a constant stress state under centrifugal loads. Twenty-five fiberglass laminated fan blades are attached to the disk with 4.87 inch diameter pins. There is a 2 inch by 6 inch shear lip where the shaft attaches to the disk. The upstream and downstream fan cavities, which surround the disk, are at different temperatures during a cryogenic run. The cavity temperatures have been measured, and the differential temperature between the two cavities is $100^{o}F$.

The shaft is a hollow forging of variable thickness and diameter along its length. The end of the shaft which connects to the disk has a 48.0 inch outer diameter and a 2.0 inch thick flange which is bolted to the disk. There are 24 - 2 inch diameter bolts which connect the flange to the disk. The shaft has a interference fit with the shear lip on the disk. To assemble the shaft and disk, the mating surfaces are first coated with a rust preventive lubricant. The coefficient of friction of the lubricant is .09, which enables very little friction to build up between the shaft and disk. Then the shaft is heated to $200^{o}F$, assembled and allowed to cool resulting in a .0035 inch shrink fit between the shaft and the shear lip of the disk. The upstream fan cavity environment is contained by a flow blocker which encircles the shaft. Between the flange and the flow blocker is the external thermal insulation and the internal thermal insulation which secures an internal shaft thermal bulkhead. The shaft, disk and bolts are made of 9% Ni with a specified yield strength of 75. ksi and a specified ultimate strength of 100. ksi.

FINITE ELEMENT MODEL

The finite element model shown in figure 2 is a one degree wedge segment of the shaft and disk with axisymmetric boundary conditions. There are 2062 nodes and 1218 elements in the model. Six rod elements connecting the shaft and disk simulate the bolted connection. The stiffness of the rod elements is 1/360 of the stiffness of all 24 bolts. The model is highly detailed in terms of fillets and contours; however, it does not contain any local bolt or pin hole details because these areas are far removed from the primary area of interest. The shaft portion of the model extends to the center-line of the bearing where it is constrained against thrust loading.

The finite element model has nonlinear contact and shear elements at the shaft-disk interface. The nonlinear contact elements are located over the entire contact surface between the shaft and the disk including the shear lip. These elements enabled the shaft to lift off or separate from the disk. The nonlinear shear elements, located only in the area of the bolt, enabled the shaft to lift off the shear lip .0035" before taking a load. This accounts for the tolerance between the bolt and the hole and the fact that the surfaces are lubricated. Also included was the shaft-to-disk shrink fit of .0035". This was accomplished by applying a -25° temperature differential between the shaft and the disk. In addition, the bolt preload of 60 ksi was included using a dislocation of .027" on the bolt elements. The above conditions can be considered initial conditions used in all load cases.

LOADS

Two basic load cases considered were: (1) a room temperature run with a drive speed of 600 rpm and (2) a cryogenic run at 360 rpm. Both cases include their appropriate fan

blade aerodynamic loads with a dynamic load factor of 1.25. The aerodynamic loads were the same as those used in the original design analysis. The 600 rpm case with its aero loads was a case by itself containing no thermal loads. The majority of the analysis was done for the 360 rpm case with its various thermal conditions necessary to evaluate the effects of retaining or removing the external thermal insulation.

For the 360 rpm case there were three basic thermal conditions that were considered; two transient conditions shown in figure 3 and a steady state condition. Case 1 transient considers a positive 85° temperature swing, and Case 2 transient considers a negative 85° temperature swing. Both cases consider a 100° temperature differential across the disk. The steady state case, as with the end of both transients, considers a $-160^{o}F$ upstream fan cavity and a $-260^{o}F$ downstream fan cavity temperature.

In addition to running the cases with and without external insulation, two other concerns were addressed: (1) with and without tip convection and (2) with and without flange conduction. Both of these address the extreme conditions for using the appropriate thermal boundary conditions. It is unknown whether the sides of the disk where the fan blades attach, convect to the free stream temperature or are insulated by the fan blades. Therefore, this area was considered with and without tip convection. It is also unknown whether the shaft flange thermally conducts to the disk through the lubricant where they are in contact. Therefore this area was evaluated for both conditions with and without flange conduction.

The heat transfer coefficients used in the analysis are a function of temperature, fan speed, and radial position from the shaft center line. During the cool down of the two transients, the coefficients were calculated using a fan speed of 120 rpm. At the

positive or negative 85° temperature swings the coefficients were calculated using a fan speed of 360 rpm. This was to simulate the actual cool-down/run process.

RESULTS

The results are described in a progressive manner. First, the initial conditions are described, then the process of determining which load case yields the maximum stress in the disk, shaft and bolts is described. Finally, the maximum stresses are determined and then compared to the allowable stresses. All of the stress contour plots are Von Mises stresses displayed on exaggerated deformed model geometry.

Figure 4 shows the effect of the shrink fit by itself and the bolt preload with the shrink fit. The stresses in the area of the bolts are local modeling stresses. This is because the structure is modeled as a one degree axisymmetric wedge which assumes that a stress variation in the circumferential direction is negligible . The shrink fit and bolt preload are viewed as initial conditions for the remaining load cases.

Figure 5 compares a 360 rpm and a 600 rpm run with no thermal load conditions. The 600 rpm case stands by itself without any thermal loadings and represents the maximum stress loading for an air mode operation. The maximum stress is found to occur on the downstream corner of the bore hole. The 360 rpm mechanical load case is the initial condition for all cryogenic temperature load cases.

Figure 6 defines the load matrix for all of the 360 rpm cryogenic load cases. The first three columns show the different boundary conditions that were considered and the last three columns show the thermal conditions that were considered. The goal was to determine the maximum stresses without external insulation and then compare these

with results from the configuration with external insulation. The numbers in the last three columns indicate the order in which the analysis progressed to determine the maximum component stresses. For all cases, a thermal analysis model was used to determine the temperature distributions which were then used as inputs to the structural model.

The first case considered was a steady state temperature case. The four combinations of thermal boundary conditions (with and without tip convection, and with and without flange conduction) were used to calculate the steady state temperatures and ultimately the stresses associated with them. These results indicated that the worse case stress was obtained using the boundary conditions of tip convection and no conduction across the flange.

The next step was to analyze the two transient thermal cases using the above thermal boundary conditions from 0 - 27,400 seconds of tunnel operation. Transient temperatures were saved every 200 seconds. The nonlinear static solutions (using all mechanical and thermal loads) were then calculated for both cases at every tenth time step where one time step was 200 seconds. At each solution step, the entire stress data set was searched for the maximum effective stress. Once the maximum stress from each block of temperatures was determined, the nonlinear static solutions were evaluated again, using every block of saved temperatures within a 5 to 10 data block bandwidth before and after the data block producing the maximum thermal stress identified in the first set of runs. This method pinpointed the actual maximum stress for each thermal transient load case. Figure 7 is a plot of the Von Mises stress in the shaft vs. time for Case 1 and Case 2. For Case 1-transient, the maximum stress occurred as the structure began to reach steady state. For Case 2-transient the maximum stress was much larger and occurred just after the -85 deg. swing in free-stream temperature.

Figure 8 is a contour plot of the maximum stresses for Case 1 at 25,400 seconds and for Case 2 at 17,000 seconds. Since Case 2-transient caused significantly higher stresses before the structure began to reach steady state, it was necessary to run the other three boundary conditions using Case 2-transient conditions to make sure the maximum stress had been determined.

Figure 9 is a temperature plot in degrees Fahrenheit of the four conditions for the Case 2 transient without external insulation. This plot shows the temperature variations with and without tip convection and flange conduction. Figure 10 is the corresponding plot of effective stress. The highest shaft stress occurred with tip convection and with flange conduction thermal boundary conditions. The highest disk stresses occurred without tip convection and without flange conduction. The highest bolt loads occurred with tip convection and without flange conduction. These stresses were then compared to the original design with external insulation.

Figure 11 is a plot of the maximum effective stress in the shaft versus time with and without external insulation. It shows the transient variation of stress when the external insulation is removed. The peak stress occurs at 17000 seconds without external insulation. The stress contours are shown in figure 12. Figure 13 shows the case for maximum disk stress with and without external insulation.

The history of the bolt loads was tabulated from all the stress runs from Case 2-transient conditions. This showed that at 27,400 sec. the bolt loads were still increasing and that the highest loads occurred with tip convection and without flange conduction. To find the maximum bolt load, the thermal conditions for this case were picked up at 27,400 seconds and the analysis was restarted and continued to 50,000 seconds. Stresses and bolt loads were calculated at numerous time steps until the bolt

load approached a steady state condition around 38,000 seconds. For comparison, the same procedure was used to trace the bolt loads using Case 1-transient conditions. The results of both series of runs are shown on figure 14. Figure 15 is a stress contour plot at steady-state thermal conditions giving the maximum bolt loads with and without external insulation.

The summary of results is shown in figure 16. It compares the stresses in the shaft, disk, and bolts with and without external insulation. In addition the stresses from the original design analysis and the allowable stresses are shown. For the shaft and disk, all stresses meet the primary stress criteria. The bolts did not meet the primary stress criteria therefore the stresses were separated into primary and secondary components and compared with appropriate allowables. The transmission torque was considered a primary stress. The preload and the shear from the thermal loads were considered as secondary stresses. For the bolt stresses in figure 16, the first stress is primary and the second stress is secondary. The bolts meet both primary and secondary stress criteria. Therefore, all three components meet the specified stress criteria with and without external insulation.

The peak stresses for each of the three components are plotted on a Modified Goodman Diagram for the appropriate material, shown in figure 17, to ensure that all components have a infinite design life. All three component stresses fell within the constant life curve indicating that the components have infinite life.

CONCLUDING REMARKS

A nonlinear finite element analysis of the shaft-disk region of a fan drive system has been performed. The analysis used nonlinear features to account for the contact

between the shaft and the disk. The analysis loads consisted of aerodynamic and centrifugal loads, thermal loads, the effects of the shrink fit between the shaft and disk, and bolt preload. Two variables in terms of boundary conditions were considered: with and without tip convection and with and without flange conduction. The maximum stresses were determined with and without external insulation on the shaft. Although the stresses were higher without external insulation, the stresses did meet all stress criteria. In addition, all stresses were within the infinite life regime of the Modified Goodman diagram. Therefore, the structural integrity of the shaft-disk region is not compromised if the external insulation is removed.

REFERENCES

1. William H. Greene and Carl E. Gray, Jr., STRUCTURAL ANALYSIS OF A THERMAL INSULATION RETAINER ASSEMBLY, NASA Technical Memorandum 101580, July 1989.

2. PATRAN Division/PDA Engineering, PATRAN Plus Users Manual Vol. 1 and 2, July 1988.

3. Whetstone, W. D., EISI-EAL Engineering Analysis Language Reference Manual EISI-EAL System Level 312. Engineering Information Systems, Inc., August 1985.

NTF Fan Region

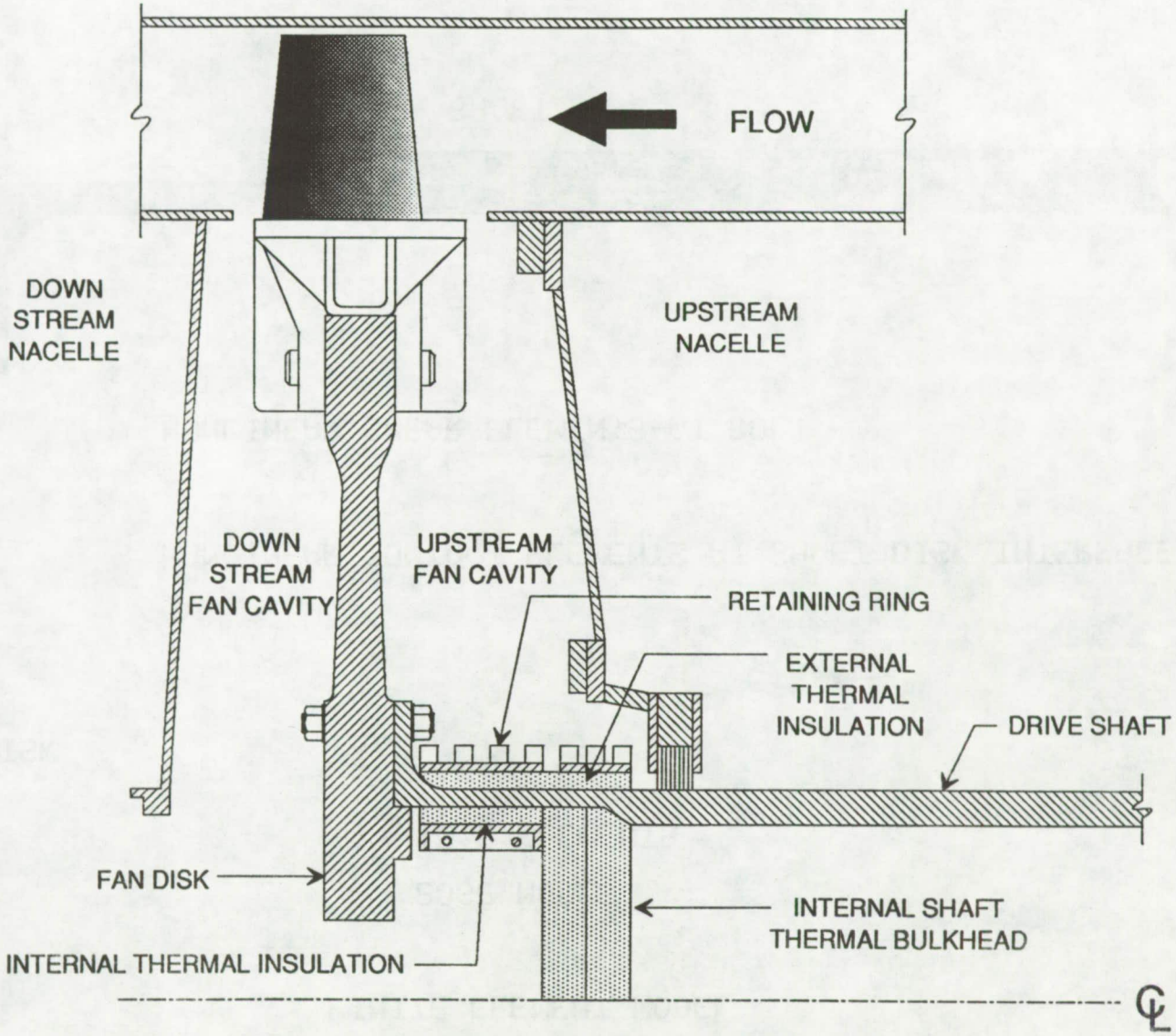

Figure 1. Cross section of NTF fan region.

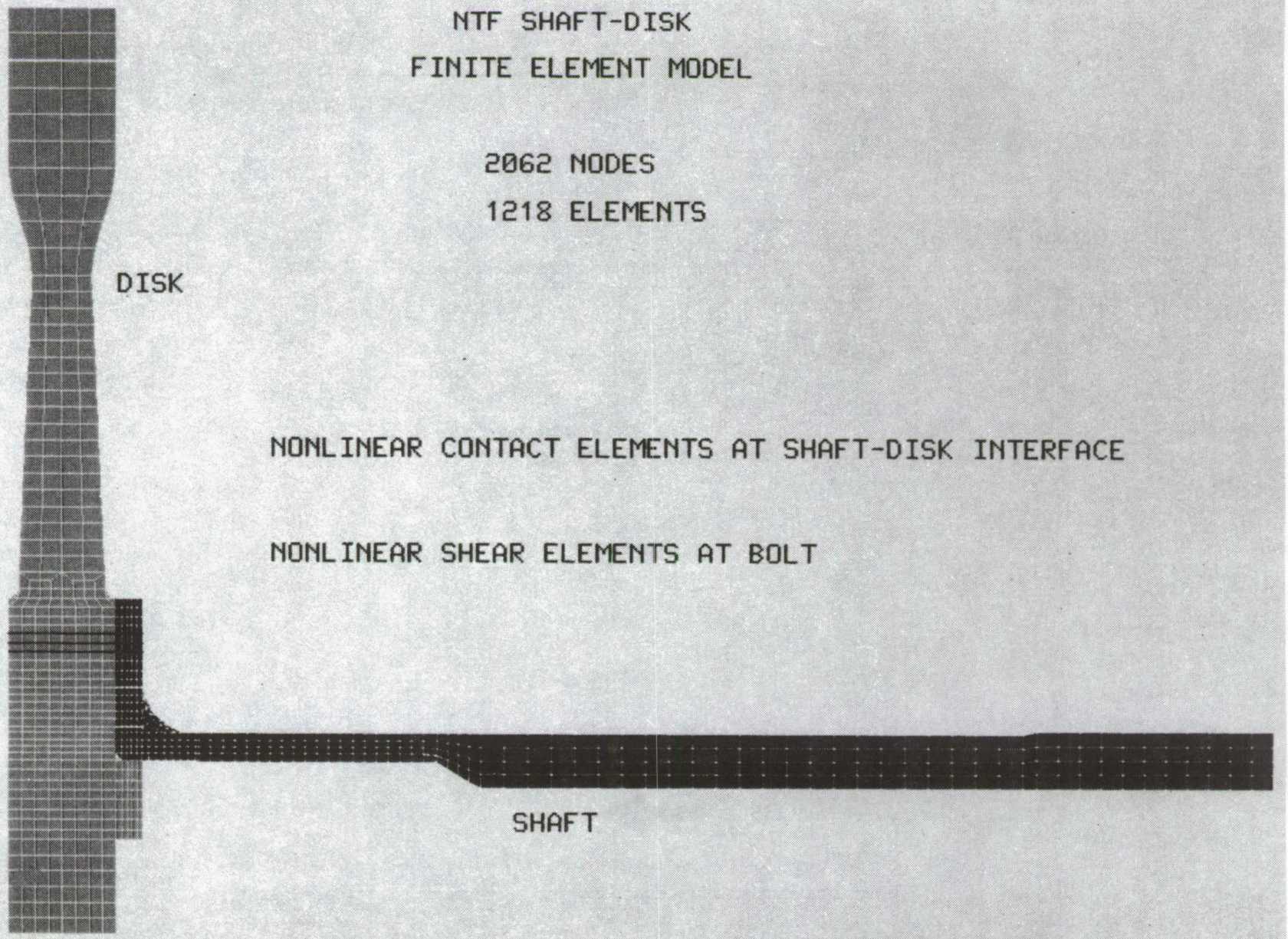

Figure 2. NTF shaft-disk finite element model.

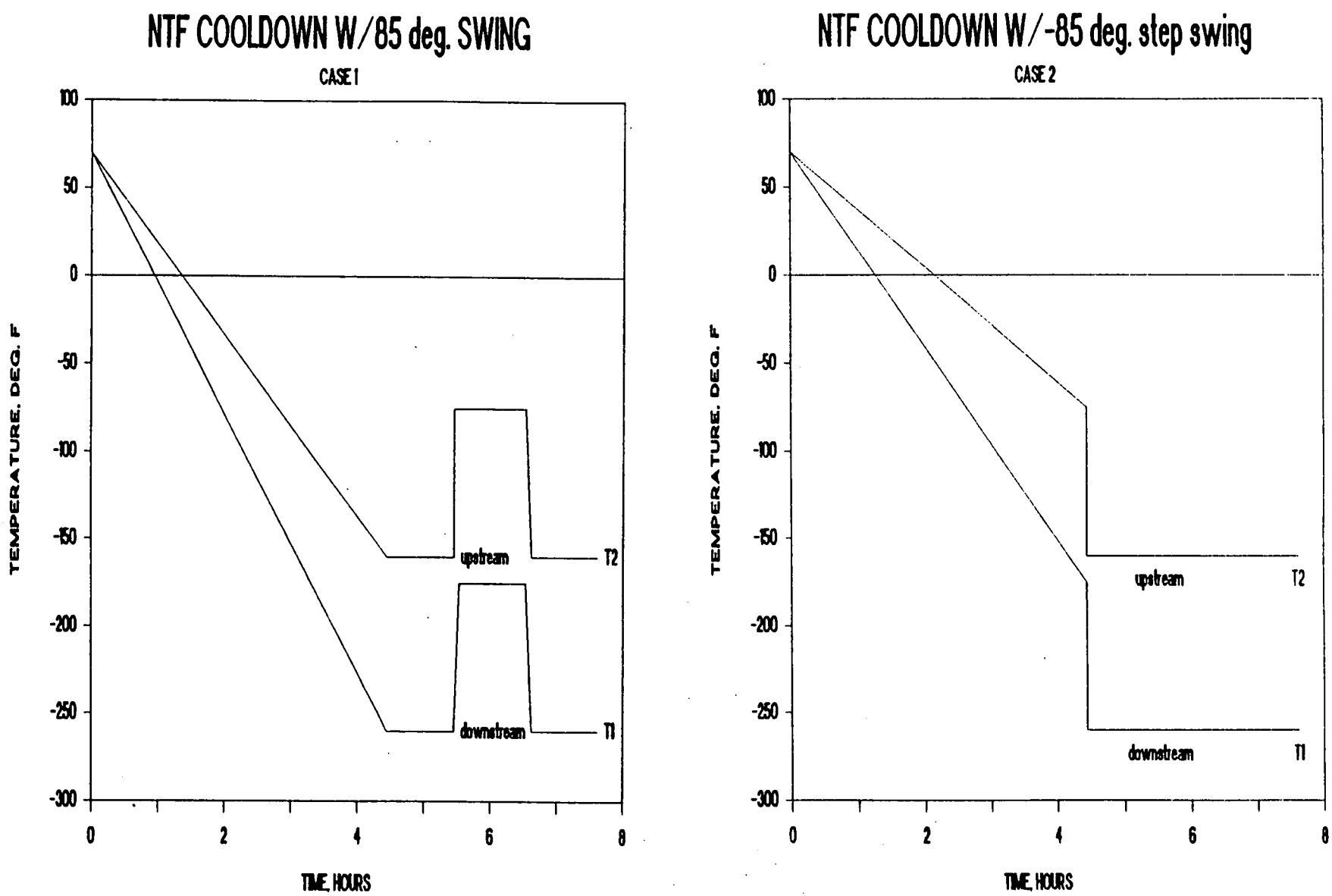

Figure 3. Upstream and downstrean fan cavity temperatures for Case 1 and Case 2 transients.

ORIGINAL PAGE IS
OF POOR QUALITY

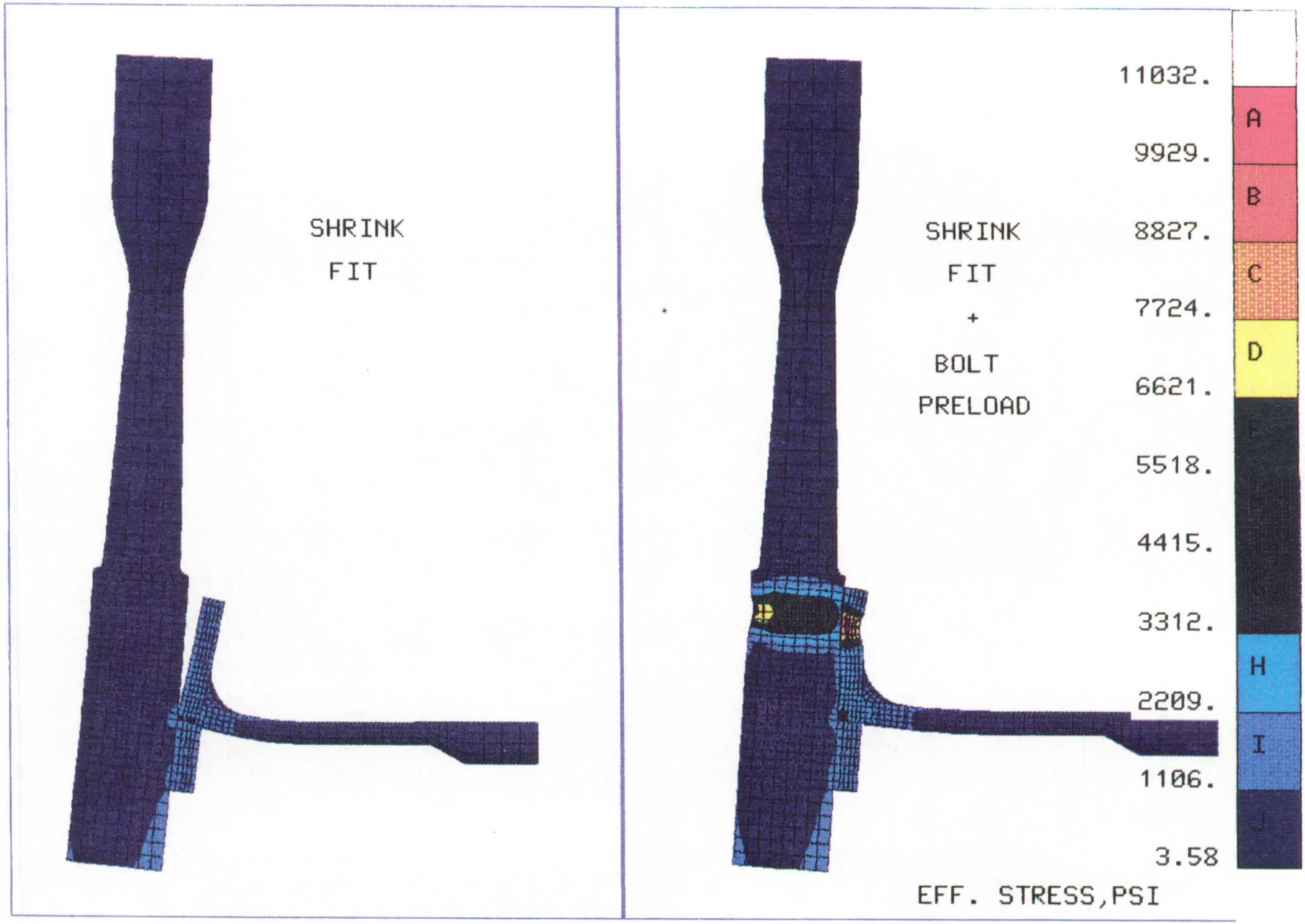

Figure 4. Stress and deformation plot of shrink fit and bolt preload.

ORIGINAL PAGE IS
OF POOR QUALITY

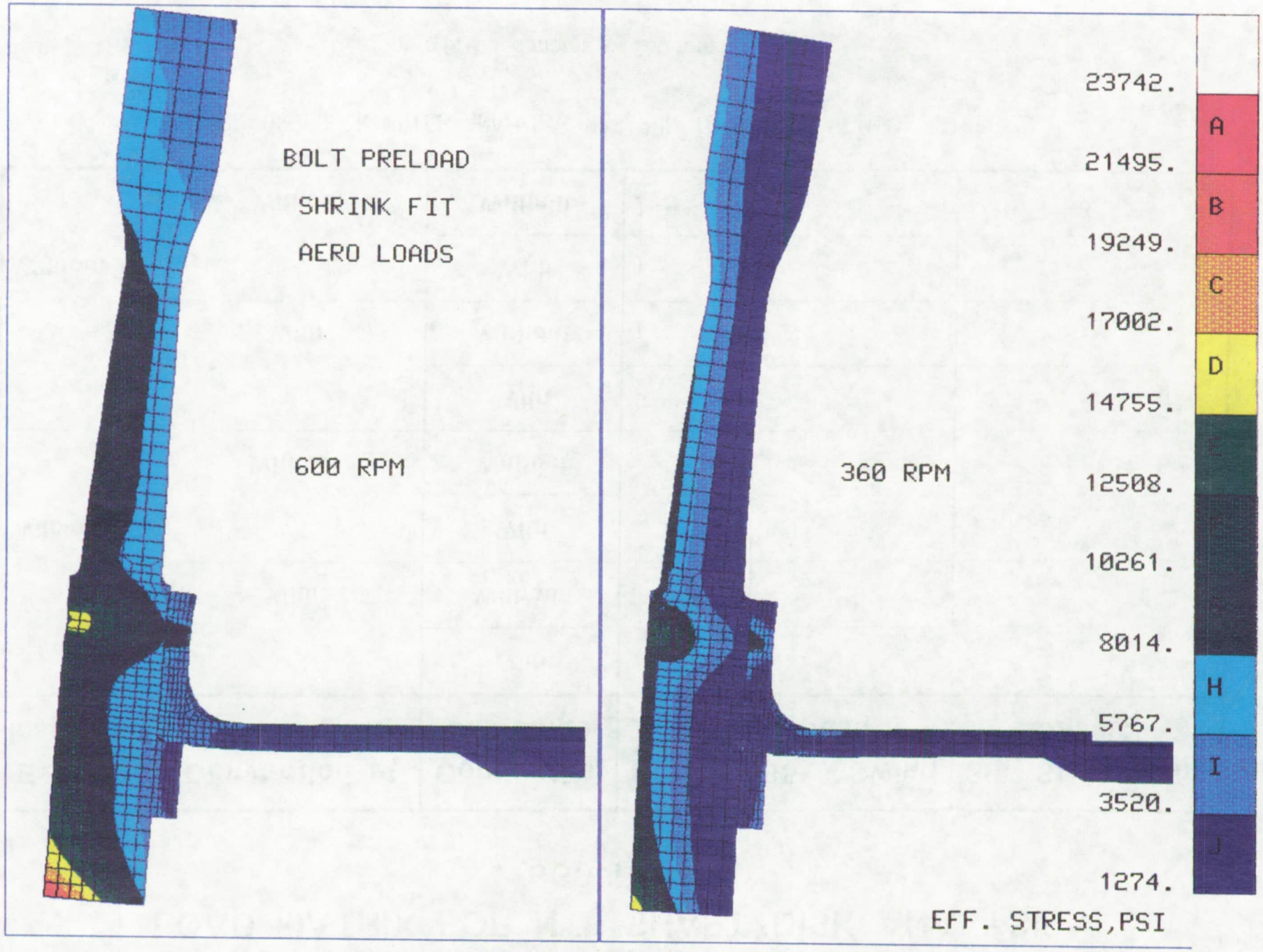

Figure 5. Stress and deformation plot of 600 rpm and 360 rpm drive speed.

ORIGINAL PAGE
COLOR PHOTOGRAPH

LOAD MATRIX FOR NTF SHAFT/DISK ANALYSIS
360 RPM

External Insulation	Convection at Blade Interface	Conduction at Flange	Steady State	85 Swing Case 1	85 Step Swing Case 2
With	With	With	7		4
		Without	6		
	Without	With			
		Without			5
Without	With	With	1		3 4
		Without	1 6	2	2 3
	Without	With	1		3
		Without	1		3 5

1,2,.... ORDER IN WHICH ANALYSIS WAS RUN TO DETERMINE MAX. STRESSES

Figure 6. Load matrix for 360 rpm load case.

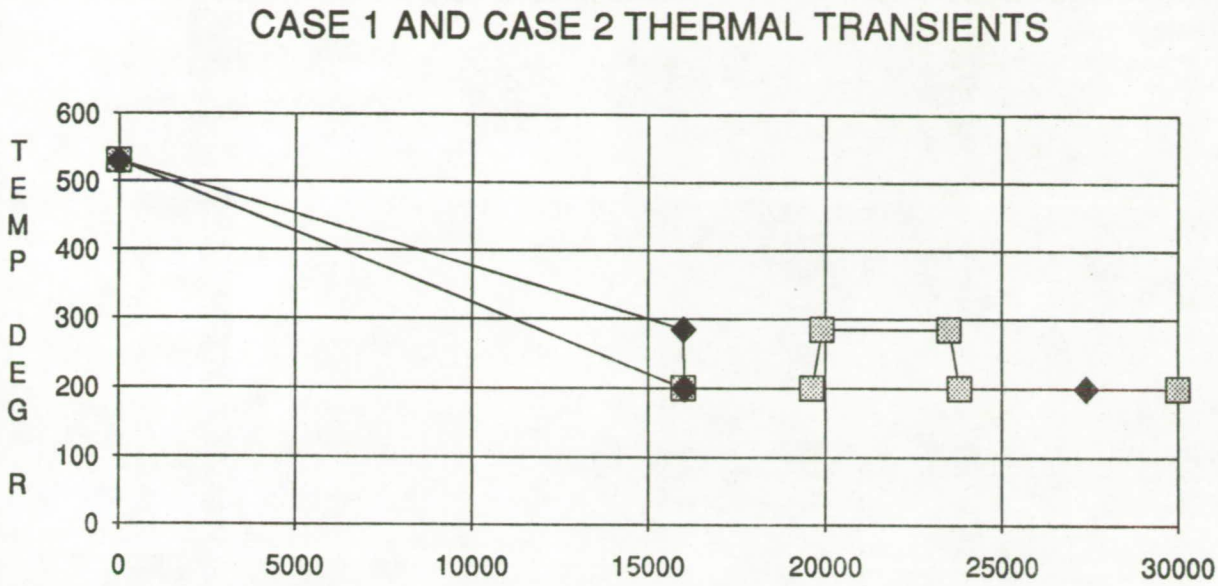

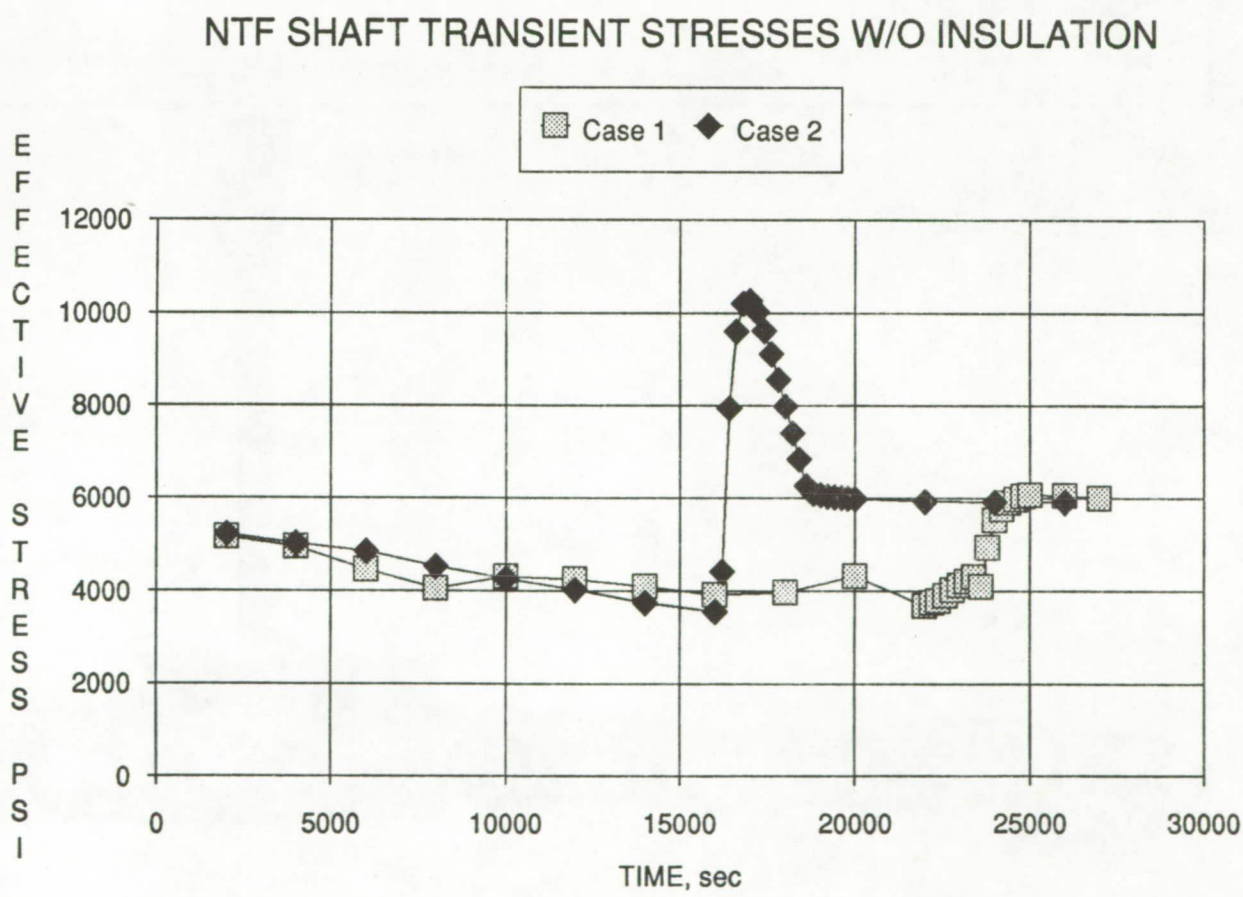

Figure 7. Effective stress on the shaft vs. time for Case 1 and Case 2 transients.

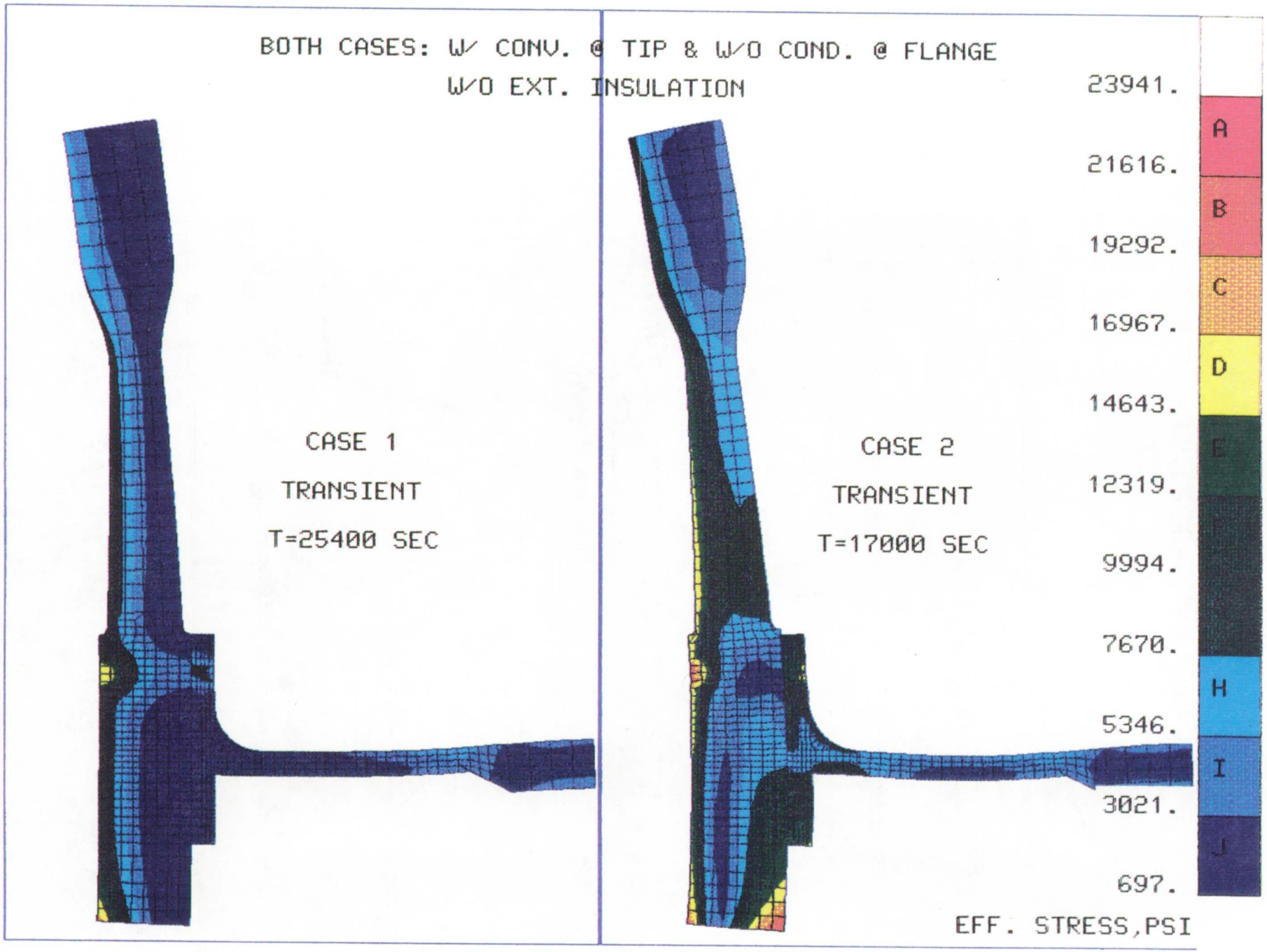

Figure 8. Stress and deformation plot of Case 1 and Case 2 transients.

ORIGINAL PAGE
COLOR PHOTOGRAPH

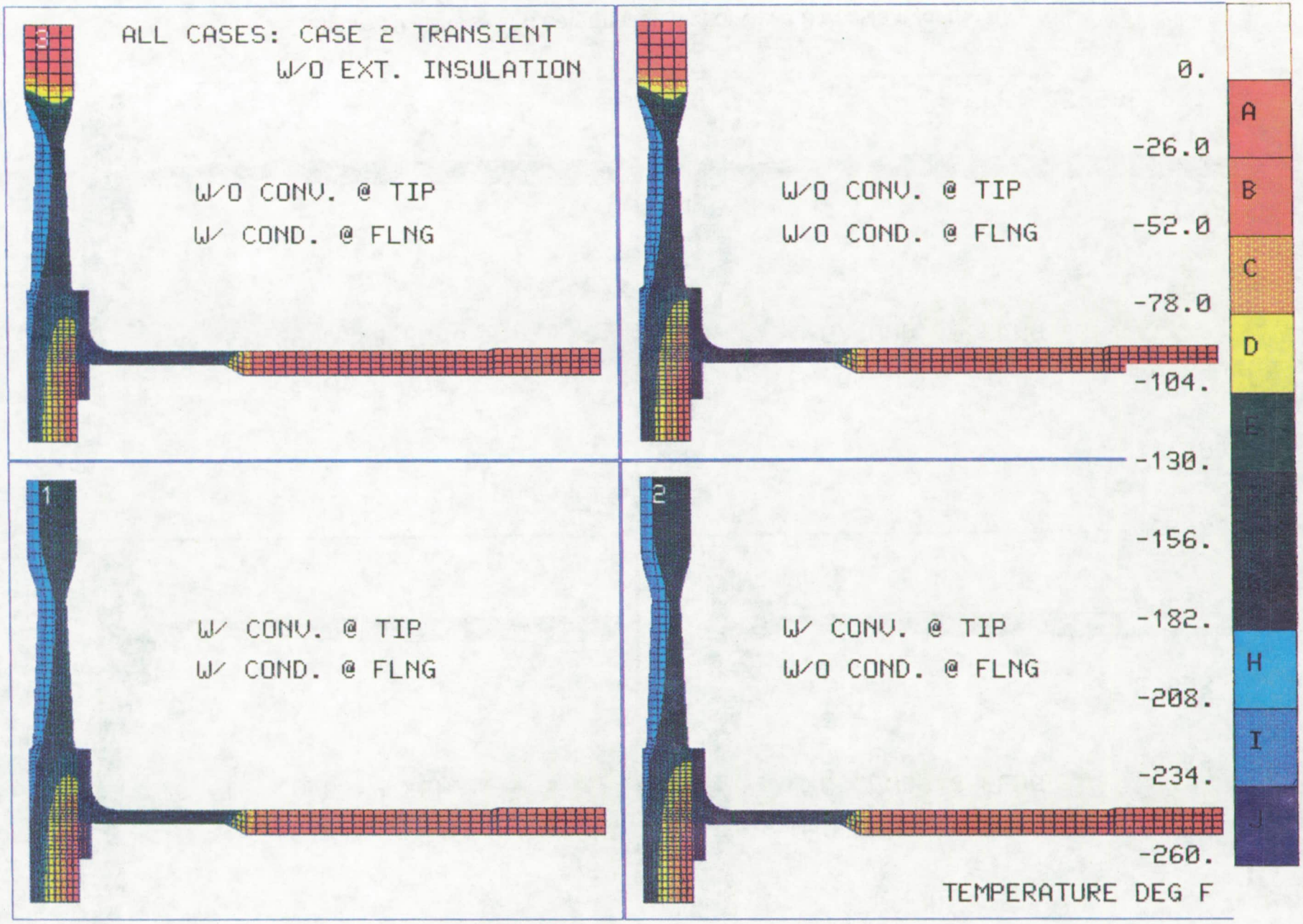

Figure 9. Temperature plot in degrees fahrenheit for Case 2 transient for the four boundary conditions.

ORIGINAL PAGE
COLOR PHOTOGRAPH

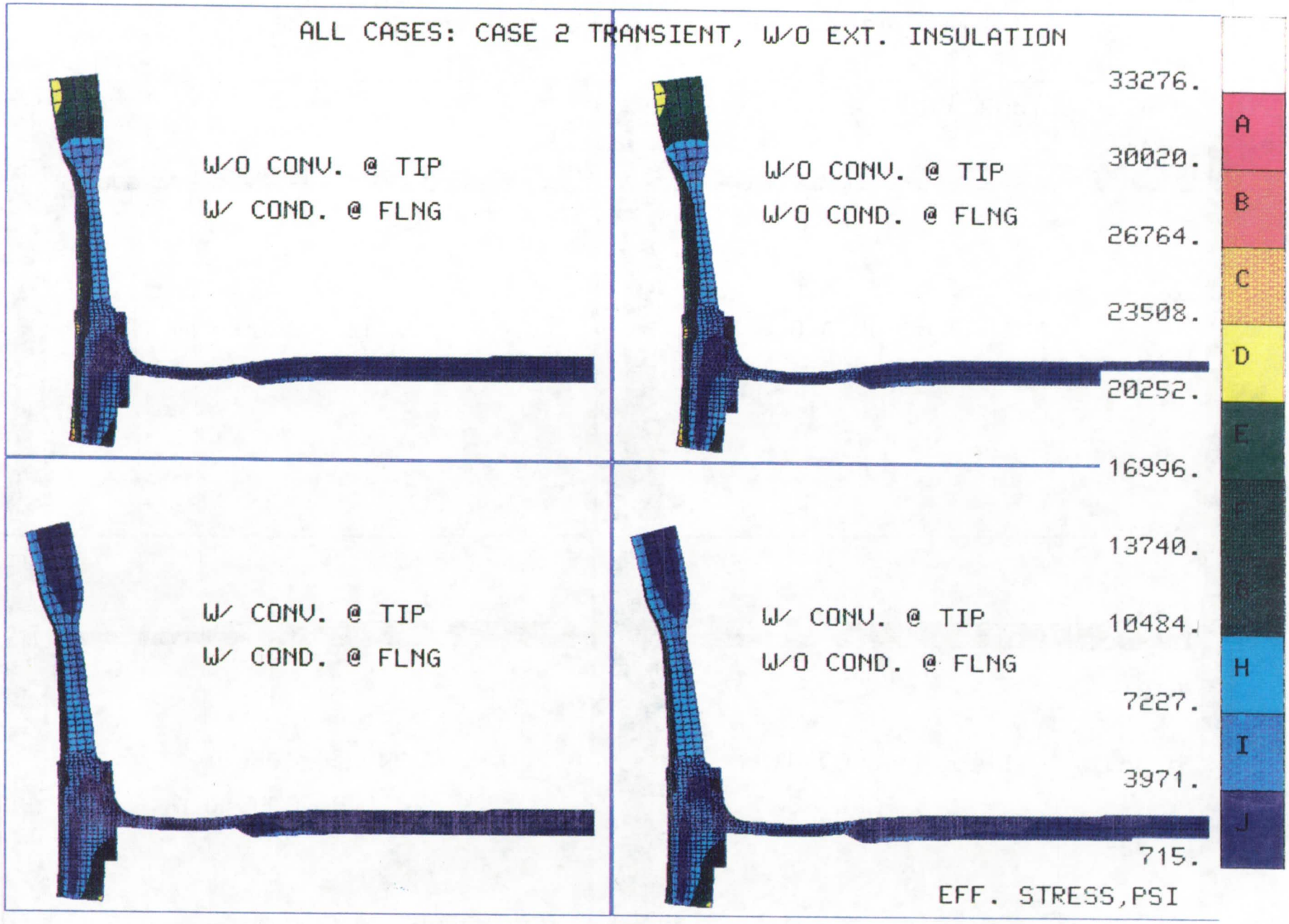

Figure 10. Stress and deformation plot of Case 2 transient for the four boundary conditions.

ORIGINAL PAGE
COLOR PHOTOGRAPH

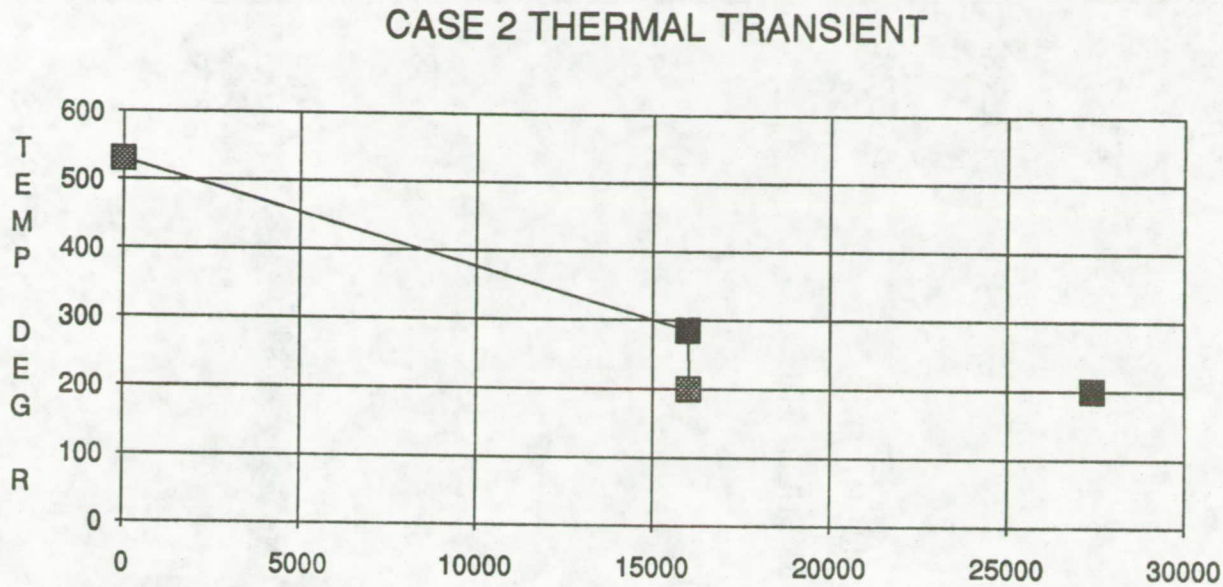

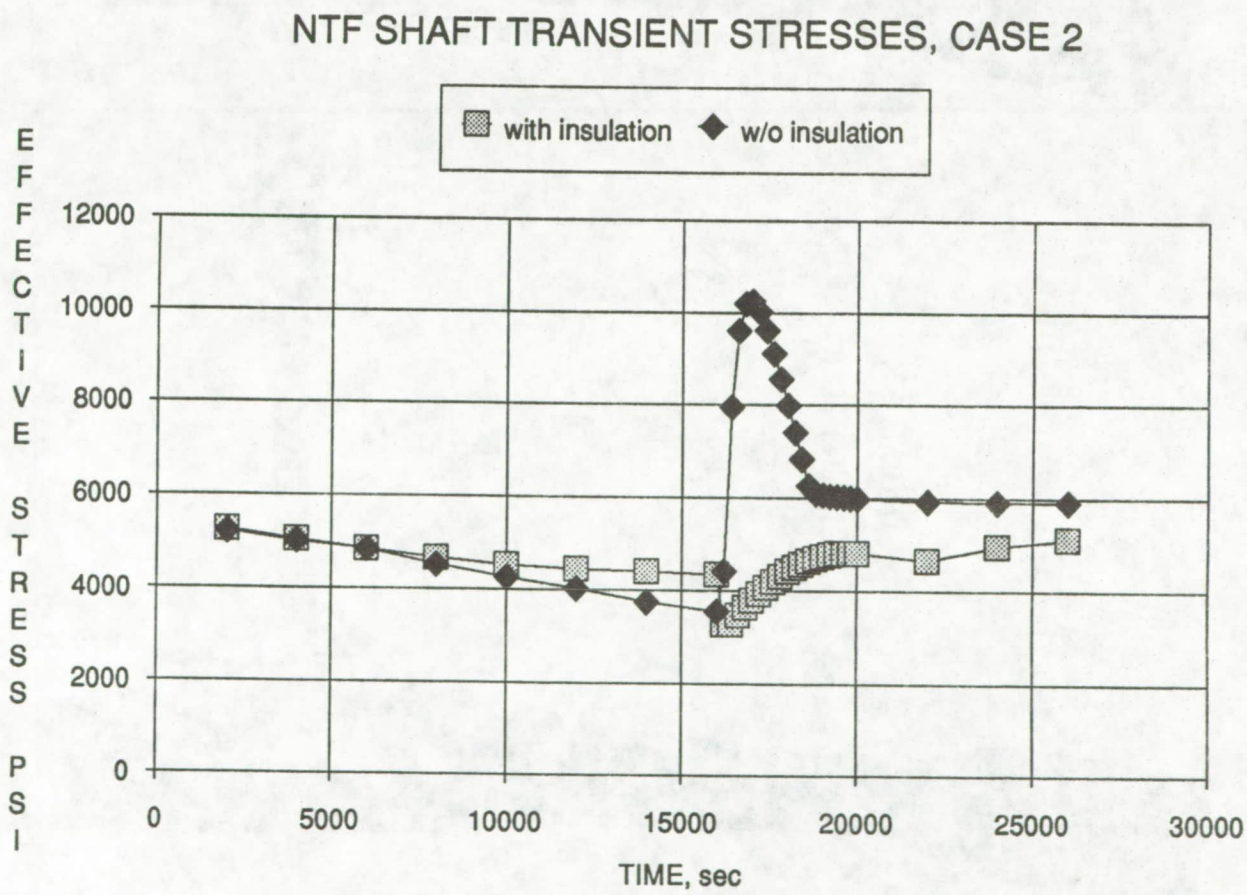

Figure 11. Effective stress on the shaft vs. time for Case 2 transient with and without external insulation.

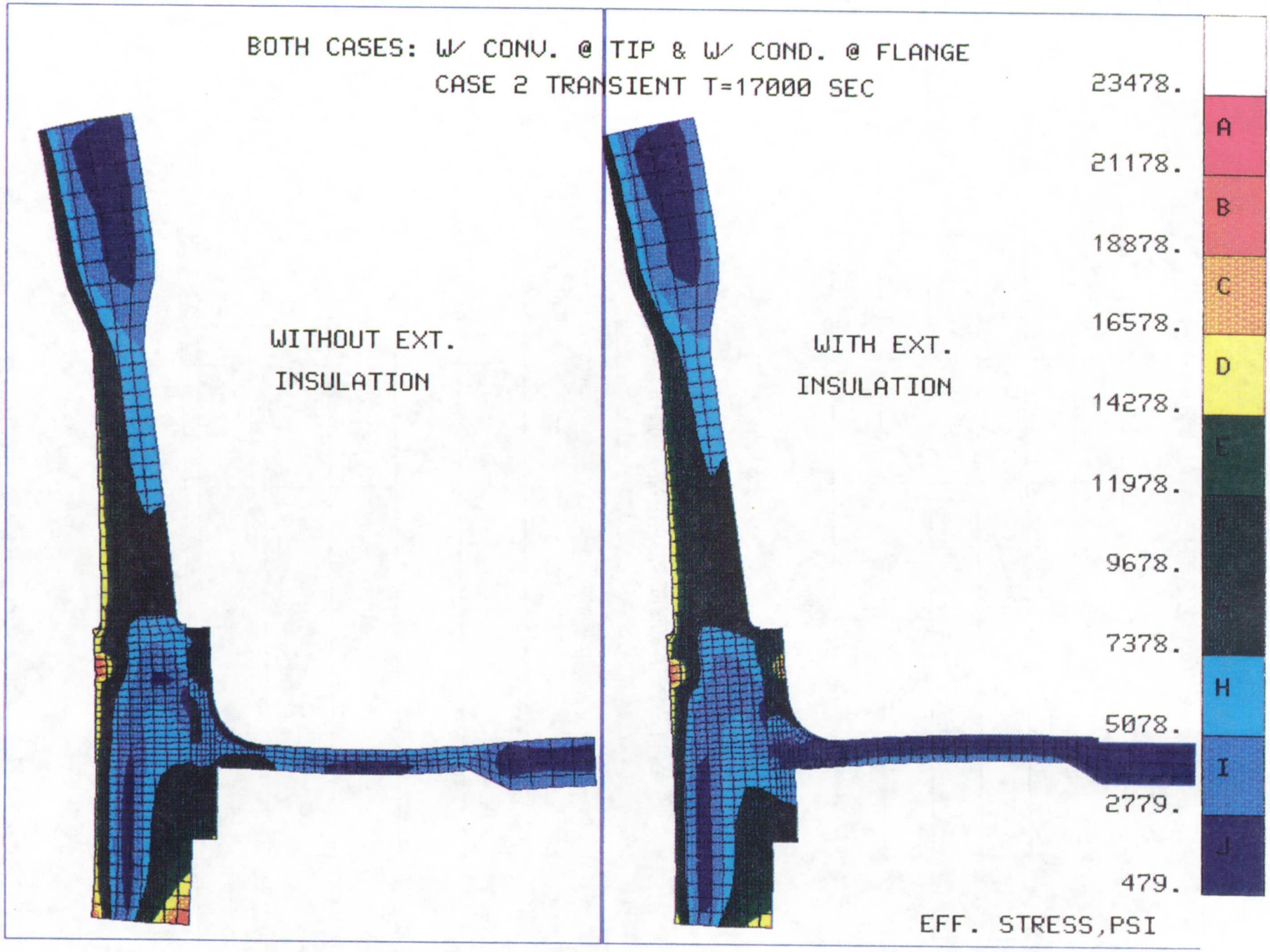

Figure 12. Stress and deformation plot for worst case shaft stress with and without external insulation.

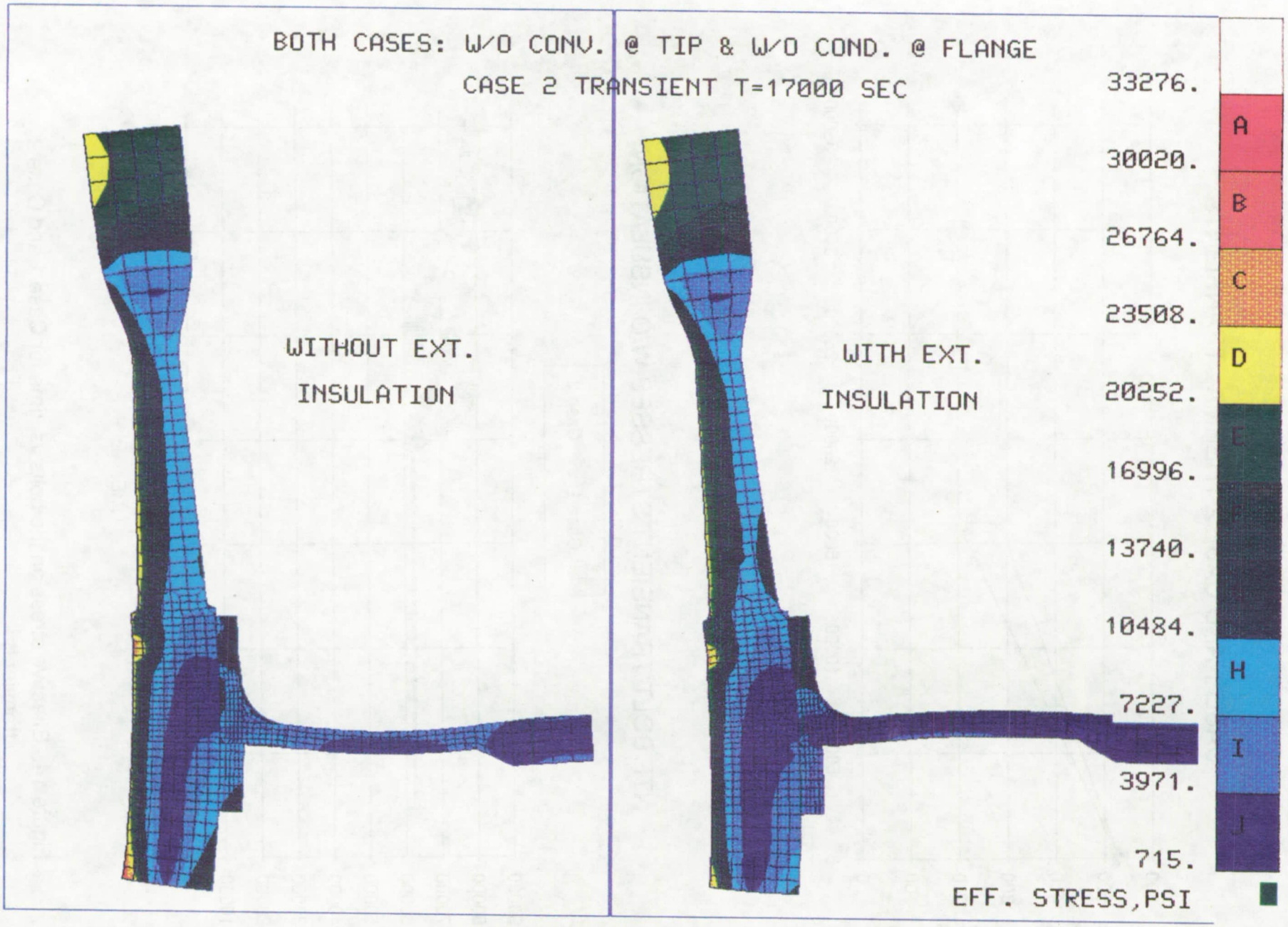

Figure 13. Stress and deformation plot for worst case disk stress with and without external insulation.

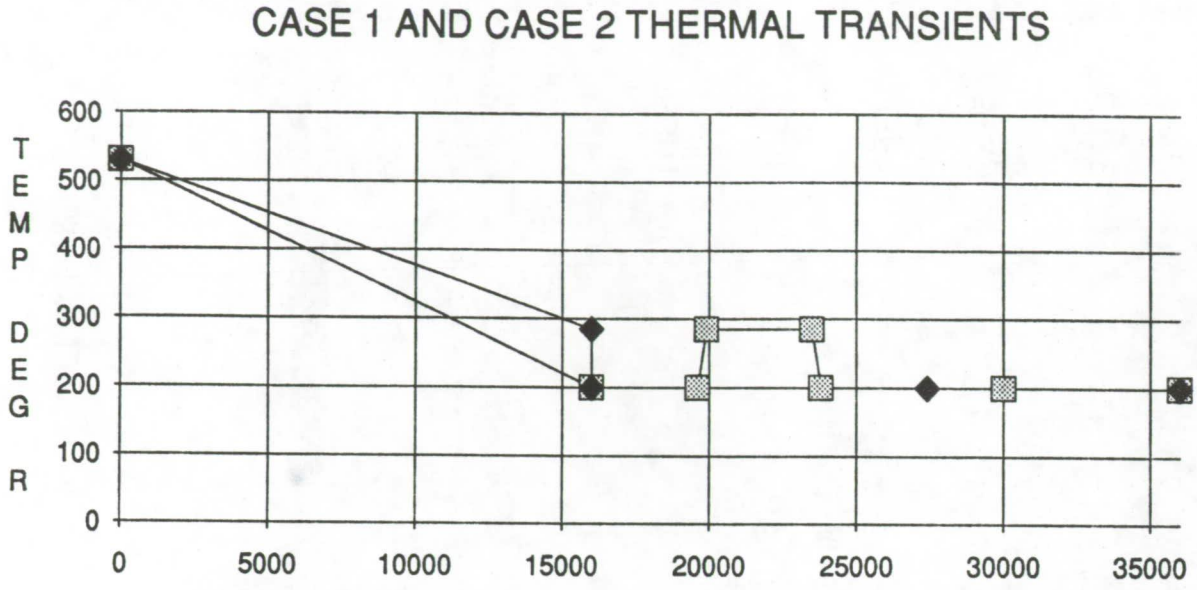

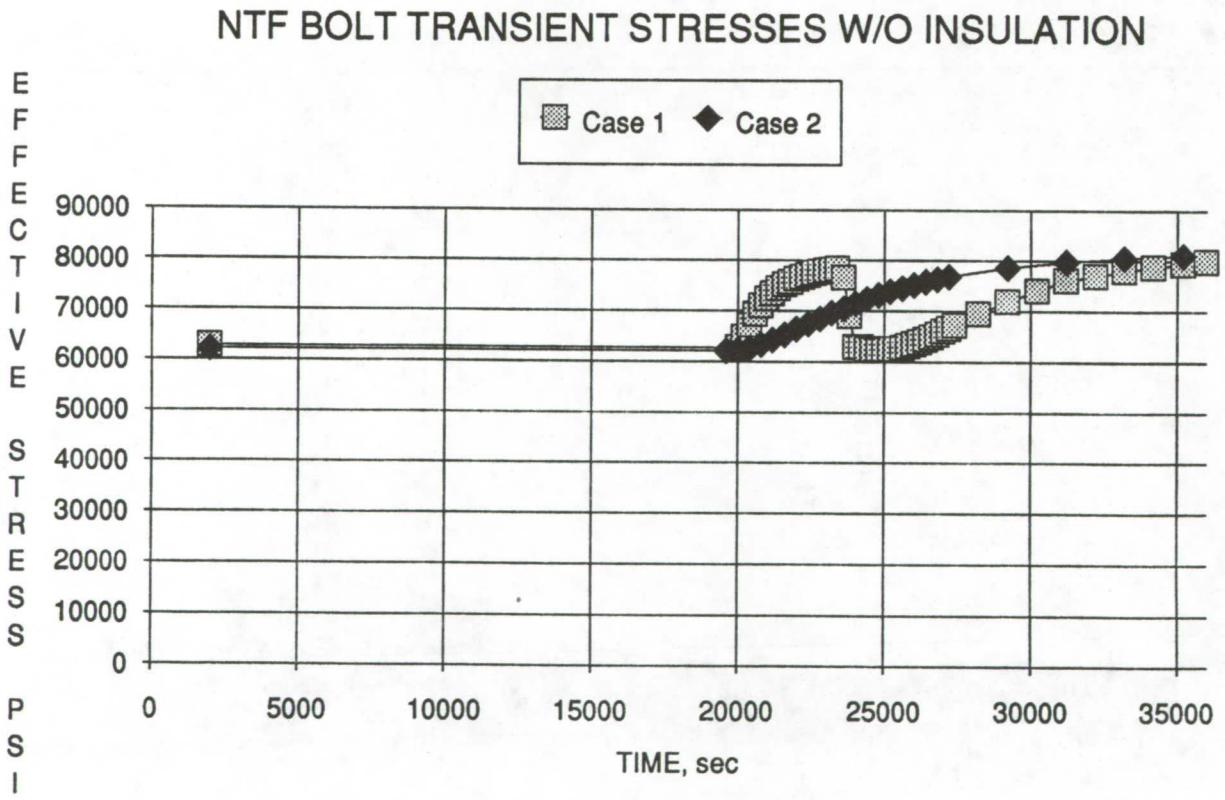

Figure 14. Effective stress on the bolts vs. time for Case 1 and Case 2 transients.

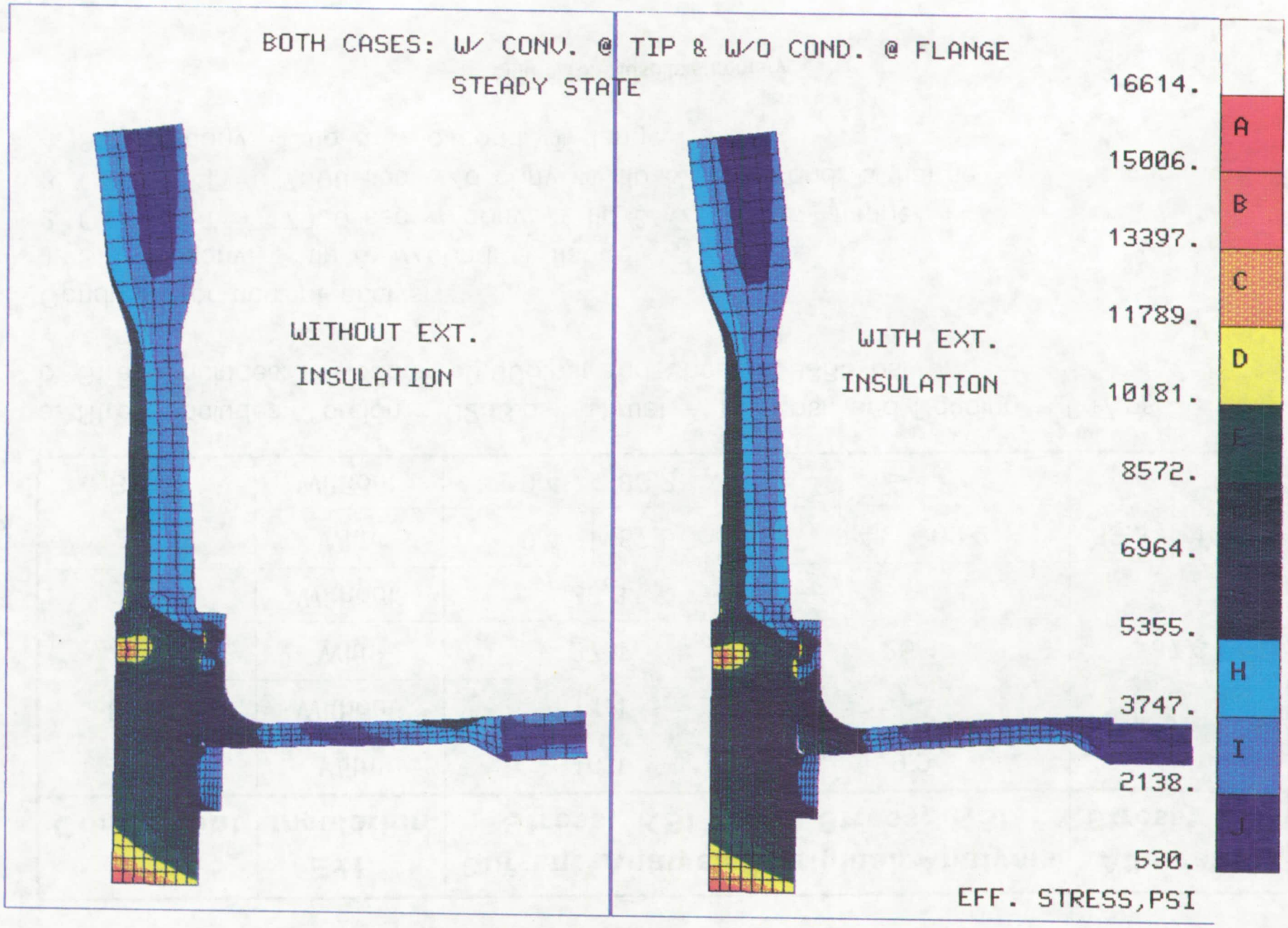

Figure 15. Stress and deformation plot for worst case bolt stress with and without external insulation.

RESULTS SUMMARY

Component	Ext. Insulation	Current Analysis Stress, KSI		Original Analysis Stress, KSI		Allowable Stress, KSI	
Shaft[a]	With[1]	10.1		9.9		37.3	
	Without[2]	14.4					
Disk	With[3]	27.4		25.1			
	Without[3]	33.3					
Bolts[b]	With[4]	9.4	87.5	9.4	62.2	33.3	100.0
	Without[4]	9.4	83.2				

a. Stress includes: Torsion = 3253.psi, Thrust = 1806.psi, and Bending = 847.psi
b. Stress includes: Preload = 60,000.psi and Shear = 9363 psi

Condition for current analysis
1. S.S. w/conv. @ tip & w/cond. @ flange
2. Case 2; T = 17000 sec w/conv. @ tip & w/cond. @ flange
3. Case 2; T = 17000 sec w/o conv. @ tip & w/o cond. @ flange
4. S.S. w/conv. @ tip & w/o cond. @ flange

Figure 16. Results summary.

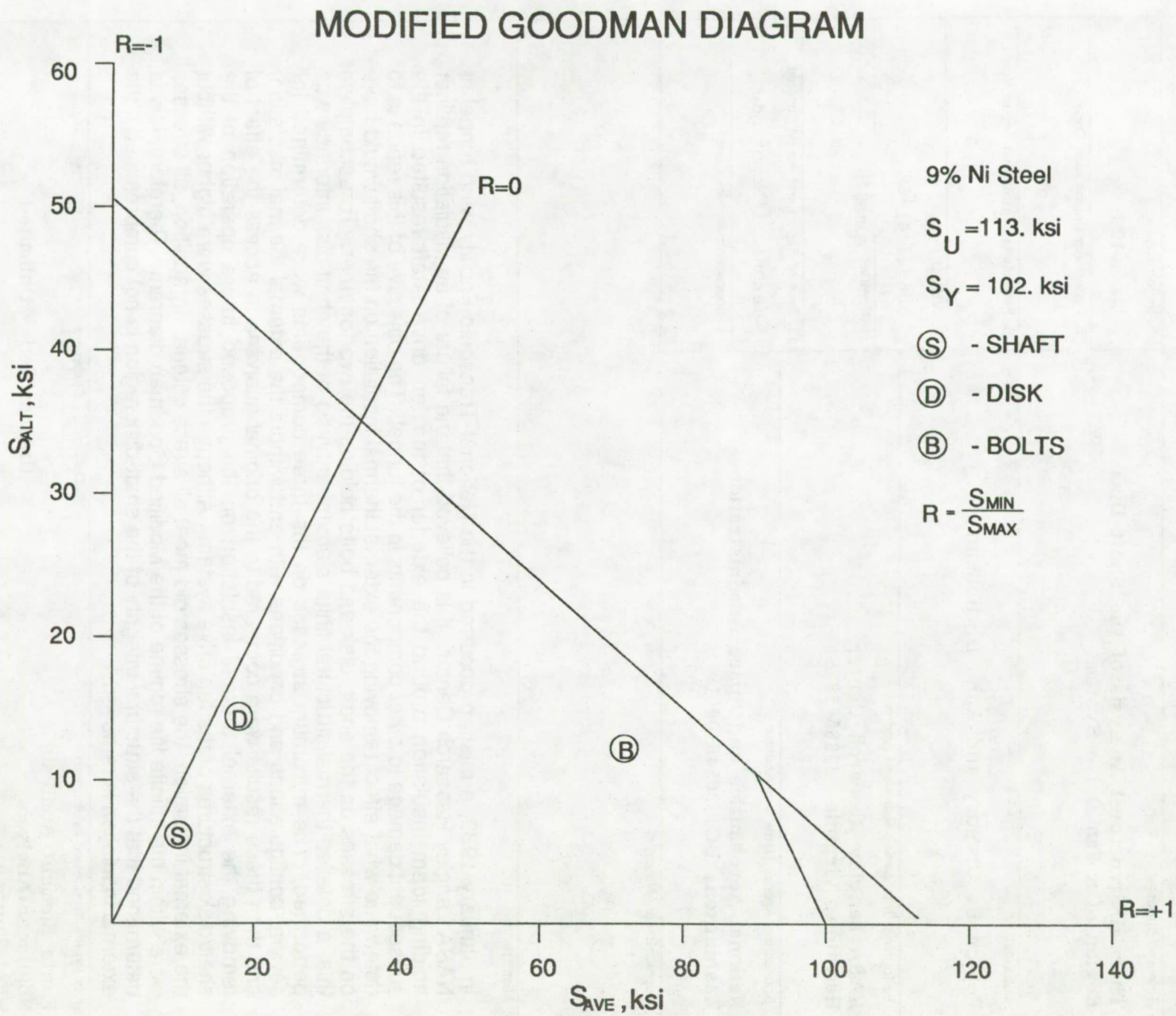

Figure 17. Modified Goodman Diagram for 9% Ni. steel.

NASA
National Aeronautics and Space Administration

Report Documentation Page

1. Report No.	2. Government Accession No.	3. Recipient's Catalog No.
NASA TM-101687		

4. Title and Subtitle	5. Report Date
Thermal/Structural Analysis of the Shaft-Disk Region of a Fan Drive System	March 1990
	6. Performing Organization Code
7. Author(s)	8. Performing Organization Report No.
Peyton B. Gregory and Anne D. Holland	
	10. Work Unit No.
	506-43-41-02
9. Performing Organization Name and Address	11. Contract or Grant No.
NASA Langley Research Center Hampton, Virginia 23665-5225	
	13. Type of Report and Period Covered
12. Sponsoring Agency Name and Address	Technical Memorandum
National Aeronautics and Space Administration Washington, DC 20546-0001	14. Sponsoring Agency Code

15. Supplementary Notes

16. Abstract

In January 1989, a mishap occurred in the National Transonic Facility wind tunnel at NASA Langley Research Center. It is believed that the failure of an insulation retainer holding foam insulation around the exterior of the fan drive shaft resulted in the subsequent damage to other components in the tunnel. The objective of this report is to determine what effect removing the external thermal insulation on the shaft would have on the stresses on the shaft, disk and bolts holding the two together. To accomplish this, a detailed thermal/structural finite element analysis of the shaft-disk interface was performed. The maximum stresses on the three components were determined for several configurations and conditions with and without the external thermal insulation, and then these results were compared to the original analyses to access the effect of removing the external thermal insulation on the proposed future operation of the shaft/disk structures of the fan drive system. Although the stresses were higher without the external insulation, the stresses did meet all stress criteria. In addition, all stresses were within the infinite life regime of the Modified Goodman diagram. Therefore, it was determined that the structural integrity of the shaft-disk region is not compromised if the external insulation is removed.

17. Key Words (Suggested by Author(s))	18. Distribution Statement
Finite Element Analysis Nonlinear Analysis Wind Tunnels	Unclassified - Unlimited Subject Category 39

19. Security Classif. (of this report)	20. Security Classif. (of this page)	21. No. of pages	22. Price
Unclassified	Unclassified	28	A03

NASA FORM 1626 OCT 86